



Comparison of UV/TiO₂ and UV/H₂O₂ processes in an annular photoreactor for removal of micropollutants: Influence of water parameters on metaldehyde removal, quantum yields and energy consumption

Olivier Autin ^a, Julie Hart ^b, Peter Jarvis ^a, Jitka MacAdam ^a,
Simon A. Parsons ^a, Bruce Jefferson ^{a,*}

^a Cranfield Water Science Institute, Department of Environmental Science and Technology, Cranfield University, Bedfordshire, MK43 0AL, UK

^b Severn Trent Water LTD., Severn Trent Centre, PO Box 5309, Coventry, West Midlands, CV3 9FH, UK

ARTICLE INFO

Article history:

Received 3 October 2012

Received in revised form 11 February 2013

Accepted 18 February 2013

Available online 28 February 2013

Keywords:

Metaldehyde

Natural organic matter

Alkalinity

Quantum yield

Advanced oxidation processes

ABSTRACT

Advanced oxidation processes have proven their efficacy in the removal of micropollutants but the role of background constituents on the kinetics of degradation is not well understood. Investigation into the role of alkalinity and background organic matter as defined by three surrogate compounds – serine, leucine and resorcinol – on the degradation of metaldehyde was conducted with a continuous flow photoreactor operated as either UV/TiO₂ or UV/H₂O₂. Background organic compounds inhibited the process through scavenging such that reaction rates were on average reduced by 19%. Modelling the radiation field enabled the quantum yield to be determined indicating that metaldehyde contributed to 0.1% of the total quantum yield under realistic background organic matter concentrations. Examination of models in term of electrical energy per order suggested that ideal reactor width of 9 mm for TiO₂ and 11.7 cm are required.

© 2013 Elsevier B.V. All rights reserved.

1. Introduction

The use of advanced oxidation processes (AOPs) for the degradation of micropollutants in drinking water applications has been successfully demonstrated at lab and pilot scale [1,2]. Existing models describing the radiation field in the reaction space have been successfully applied for the degradation of single component and even multicomponent mixtures of organic contaminants in laboratory grade water in annular photoreactors [3–6]. However, most of these studies excluded the presence of natural scavengers such as natural organic matter (NOM) or carbonate ions which have shown inhibitory effects in AOPs [1,7] resulting in over-prediction of the destruction rates [8]. Previous work at bench scale has demonstrated that the high concentration of organic and carbonate scavengers commonly present in background water reduces the proportion of available •OH that reacts with the target micropollutant down to less than 0.05% of those produced [9]. Incorporation of this impact has enabled effective prediction of the degradation of micropollutants in a UV/H₂O₂ pilot plant [8]. In such work it is

common to use measurements of the bulk NOM concentration such as absorbance at 310 nm restricting understanding on the impact of organic character on the process. The organic make-up of the background NOM is known to be highly variable and the impact of this on the degradation of micropollutants at bench scale has revealed that both the concentration and character of the organics is important through their combined impact on the overall scavenging rate [9]. The impact of NOM was shown to be common across AOPs but specific issues in relation to alkalinity were observed only with UV/TiO₂ where loss of reactive surface area due to catalyst aggregation was observed in the presence of alkalinity.

The current study aims to incorporate such findings at pilot scale in order using the previously developed model by Li Puma et al. [5] to evaluate the potential of AOPs for micropollutant removal. The work extends previous studies by directly comparing two AOPs: UV/H₂O₂ and UV/TiO₂ in order to establish process specific features and their impact on the overall suitability of the technology for micropollutant removal.

For both processes, the local volumetric rate of photon absorption (LVRPA) which informs how and where the reactions occur in the reactor was determined. From the LVRPA and experimental data, the quantum yields and energy requirement were determined for the different scenarios. Finally, the rate constants independent

* Corresponding author. Tel.: +44 1234 754813; fax: +44 1234 751671.

E-mail address: b.jefferson@cranfield.ac.uk (B. Jefferson).

Nomenclature

a	model parameter SFM
b	model parameter SFM
c_{cat}	photocatalyst concentration (kg m^{-3})
C_i	metaldehyde or NOM surrogate concentration (mol m^{-3})
C_{0i}	initial concentration of metaldehyde or NOM surrogate (mol m^{-3})
H	length of the reactor (m)
I	radiation intensity (or radiative flux) (W m^{-2})
k_T	kinetic rate constant independent of radiation absorbed ($\text{m}^3 \text{e}^{-1}$)
L	lamp length (m)
VRPA	volumetric rate of photon absorption (W or e s^{-1})
LVRPA	local volumetric rate of photon absorption (W m^{-3} or $\text{e s}^{-1} \text{m}^{-3}$)
m	order of the reaction with respect to the LVRPA
p_b	probability of scattering in the backward direction
p_f	probability of scattering in the forward direction
p_s	probability of scattering in the side direction
r	radial coordinate (m)
r^*	dimensionless radial coordinate ($=r/R$)
r_l	lamp radius (m)
r_i	reaction rate with respect to substrate I ($\text{mol s}^{-1} \text{m}^{-3}$)
R	external radius of annulus (m)
S_l	radiation emission of lamp per unit time per unit length (W m^{-1})
t	time (s)
V_t	total volume of fluid in recirculation system (m^3)
V_r	reactor volume (m^3)
z	axial coordinate (m)
z^*	dimensionless axial coordinate ($=z/H$)

Greek letters

α	geometrical parameter ($=H/L$)
β	geometrical parameter ($=L/\eta R$)
γ	dimensionless parameter SFM
δ	reaction space radial coordinate (m)
δ^*	dimensionless reaction space radial coordinate ($=\zeta/\delta$)
η	ratio of internal radius to external radius of annulus
κ	specific mass absorption coefficient at 254 nm ($\text{m}^2 \text{kg}^{-1}$)
λ	radiation wavelength (m)
σ	specific mass scattering coefficient at 254 nm ($\text{m}^2 \text{kg}^{-1}$)
τ	optical thickness
τ_{app}	apparent optical thickness
Φ	quantum yield (mol e^{-1})
ω	scattering albedo ($=\sigma/\sigma + \kappa$)
ω_{corr}	corrected scattering albedo SFM

of photon absorption were determined for both systems in order to standardize them to any reactor configuration.

2. Material and methods

2.1. Chemicals

Metaldehyde, serine, leucine, hydrogen peroxide (35% w/w), NaHCO₃ were obtained from Fisher Scientific (Loughborough, UK) and resorcinol from Sigma-Aldrich (Poole, UK) at analytical purity

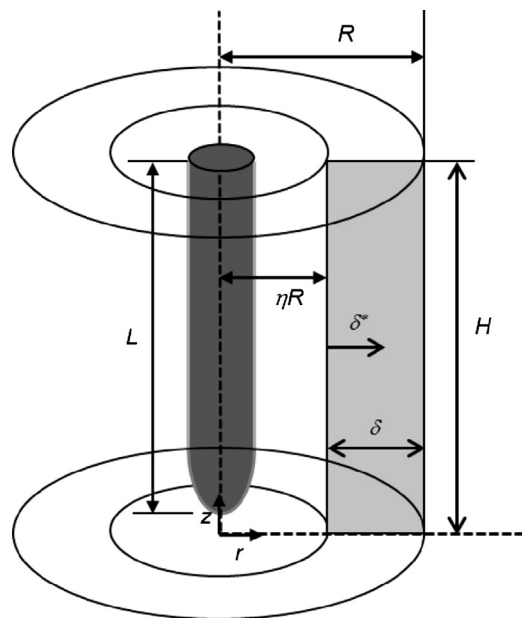


Fig. 1. Schematic representation of the geometry of the annular photoreactor.

or above. The chemical and photochemical properties of metaldehyde and the three NOM surrogates are presented in Table 1. Titanium dioxide P25 Degussa was purchased from Lawrence Industries (Tamworth, UK). Laboratory grade water (LGW) was produced by a Purelab Option (S7/15, 18.2 MΩ and TOC < 3 ppb). The surface water was collected post-GAC from a drinking water treatment works in the Severn Trent Water region, UK and had a DOC of 3.5 mg L⁻¹ and an alkalinity of 120 mg L⁻¹ as CaCO₃. The water was stored in the dark at 4 °C until used for experiments.

2.2. Photoreactor

The system comprised a holding tank and an annular photoreactor. The solution and TiO₂ or H₂O₂ were mixed together in the holding tank and left in contact for 30 min before irradiation. The mixture was then pumped (520 U, Watson Marlow) into the reactor in an up flow mode. Air was sparged co-currently in the reactor in order to have a good mixing and to enhance the TiO₂ photocatalytic process by trapping the e⁻ formed at the surface. The outer wall of the reactor is made of stainless steel with an internal diameter of 0.077 m, and the inner wall consists of a quartz tube (external diameter 0.047 m) mounted at the axial centre of the reactor (Fig. 1). The dimensions of the reactor are presented in Table 2. The light source was a Trojan 45 W UVC lamp emitting at 253.7 nm which was inserted inside the quartz tube. The photon flux was measured using a microprocessor-controlled radiometer (Cole-Parmer) fitted with a 254 nm UVC sensor, and was found to be 141 W m⁻².

The optical properties of TiO₂ were determined for the specific conditions of mixing and particle aggregation of this study. The sum of absorption and scattering coefficients corresponds to the extinction coefficient which can be determined spectrophotometrically [13]. The extinction coefficient was 3640 and 314 m² kg⁻¹ in the presence and in the absence of alkalinity respectively. Salaices et al. [14] observed that although an increase of particle agglomerate sizes leads to smaller extinction coefficients at a given wavelength, it had the same effect on both the scattering and absorption coefficient. In other words, for a given wavelength, the scattering albedo ($\sigma/\sigma + \kappa$) can be assumed constant, and therefore, the ratio of 0.4 determined by Li Puma et al. [15] for a low pressure lamp irradiating at 253.7 nm was used in this study.

Table 1

Photochemical and chemical properties of metaldehyde and the three NOM surrogates.

	Metaldehyde	Serine	Leucine	Resorcinol
ζ ($M^{-1} \text{cm}^{-1}$)	19.0	0.3	0.5	559.8
Concentration (M)	5.68×10^{-8}	1.89×10^{-5}	1.89×10^{-5}	1.89×10^{-5}
$k_{\cdot\text{OH}}$ ($M^{-1} \text{s}^{-1}$)	1.3×10^9 [9]	3.2×10^8 [10]	1.7×10^9 [10]	1.1×10^{10} [11]
Log k _{ow}	0.12 [12]	-3.07 [12]	-1.52 [12]	0.80 [12]

2.3. Irradiation procedures

Stock solutions of leucine, serine and resorcinol were prepared in LGW at 500 mg L^{-1} , and metaldehyde at 1 mg L^{-1} . In order to accurately follow the degradation of metaldehyde, an initial concentration of $10 \mu\text{g L}^{-1}$ ($5.68 \times 10^{-8} \text{ M}$) was chosen and a DOC concentration of 3.5 mg L^{-1} was used so that the molar ratio between metaldehyde and the NOM surrogates was 1:1000 with equimolar concentrations of serine, leucine and resorcinol (DOC concentrations of 0.9, 1.7 and 0.9 mg CL^{-1} respectively). When the influence of alkalinity was tested, NaHCO_3 was added so that the alkalinity was 120 mg L^{-1} as CaCO_3 . 10 L of solution was freshly prepared before each test by spiking the required volume of each stock solution in LGW. Experiments were carried out at natural pH and at room temperature ($20\text{--}22^\circ\text{C}$). The residence time was controlled by adjusting the flow rate and samples were taken at the outlet of the reactor when the required irradiation time was reached. The concentrations of oxidants were fixed at 100 mg L^{-1} and 8 mM for TiO_2 and H_2O_2 respectively as found to be optimum concentrations for this application [16]. Such a high concentration of hydrogen peroxide is unlikely to be used in industrial applications but greatly increased the reaction rate and was used in order to compare the two processes at their optimum potential.

2.4. Sample analysis

For UV/ TiO_2 , samples were filtered through $0.45 \mu\text{m}$ syringe filters (Millex-HA) to separate the suspended TiO_2 prior to analysis. The analyses were performed using a Waters 2695 LC system coupled with a Waters Quattro Premier Xe MS-MS. The aqueous mobile phase A consisted of 5 mM ammonium acetate/0.1% formic acid and the organic mobile phase B was acetonitrile/0.1% formic acid. The flow rate was set to 0.2 mL min^{-1} and the conditions were 50% A and 50% B held for 2 min. The Quattro Premier Xe tandem quadrupole mass spectrometer was operated under positive electrospray ionization mode for metaldehyde, leucine and serine and negative electrospray ionization mode for resorcinol. The instrument was operated in multiple reaction monitoring set to monitor ions m/z 194, m/z 131.7, m/z 105.7 and m/z 108.5 for metaldehyde, leucine, serine and resorcinol respectively. Source conditions

Table 2Optical parameters of TiO_2 and H_2O_2 solutions and system parameters.

Model parameter	UV/ TiO_2	UV/ H_2O_2
Reactor length, H	0.38 m	0.38 m
Lamp length, L	0.36 m	0.36 m
Gap size, δ	0.015 m	0.015 m
Geometrical parameters	$\alpha = 1.056$, $\beta = 15.329$	$\alpha = 1.056$, $\beta = 15.329$
Specific absorption coefficient, κ	$2184^{\text{a}}/188.4^{\text{b}}$ $\text{m}^2 \text{kg}^{-1}$	
Specific scattering coefficient, σ	$1456^{\text{a}}/125.6^{\text{b}}$ $\text{m}^2 \text{kg}^{-1}$	
Scattering albedo, ω	0.4	
Optical thickness, τ	423	
[absorbing species]	100 mg L^{-1}	0.008 M
Decadic molar absorption coefficient, ξ	$2255 \text{ M}^{-1} \text{ cm}^{-1}$	$19.6 \text{ M}^{-1} \text{ cm}^{-1}$

^a The absence of alkalinity.^b The presence of alkalinity.

were as follows: capillary 3.5 kV , source temperature 120°C , desolvation temperature 350°C , and nitrogen drying gas 1000 L h^{-1} . Calibrated curves were generated prior to each new sequence and the concentrations were determined using Micromass QuantLynx.

The decadic molar absorption coefficient was defined using:

$$A_{254,i} = \xi_i \times l \times C_i \quad (1)$$

where $A_{254,i}$ is the absorbance of i at 254 nm (in cm^{-1}), ξ_i is the decadic molar absorption coefficient of i at 254 nm (in $\text{M}^{-1} \text{ cm}^{-1}$), l is the path length in the spectrophotometer (1 cm) and C_i is the concentration of i (in M).

2.5. Description of the model used

In AOPs, the quantum yield evaluates the efficiency of a process and is defined as:

$$\phi = \frac{\text{total number of moles of pesticide transformed}}{\text{total number of moles of photons absorbed in the system}} = \frac{V(dC_i/dt)_{t=0}}{\text{VRPA}} \quad (2)$$

where $(dC_i/dt)_{t=0}$ is the initial rate of degradation of compound i (in M s^{-1}), V is the volume of the reactor (in L) and VRPA is the volumetric rate of photon absorption (in e s^{-1}).

The VRPA, defined as the photon energy absorbed at a specific position in the reaction space [15] can be estimated by integrating the local volumetric rate of photon absorption (LVRPA) throughout the entire reactor volume, such as:

$$\text{VRPA} = \int_{V_r} (\text{LVRPA}) dV_r \quad (3)$$

$\text{UV/H}_2\text{O}_2$ is a homogeneous system and the photons are absorbed by all the species in solution whilst UV/TiO_2 is a heterogeneous system and the photons are absorbed by both the photocatalyst and the species in solution. For both processes, the concentration of $\cdot\text{OH}$ precursor ($\text{TiO}_2/\text{H}_2\text{O}_2$) is much larger than that of the organic compounds. For UV/TiO_2 , more than 99.5% of the photons are absorbed by TiO_2 (absorption coefficient $\kappa_{\text{TiO}_2} = 2.82 \text{ cm}^{-1}$ compared to $\kappa_{\text{all other species}} = 0.0106 \text{ cm}^{-1}$) and the contribution from the organic compounds to the LVRPA can be safely neglected. For $\text{UV/H}_2\text{O}_2$ due to the low absorption of light at 254 nm by H_2O_2 , the fraction of photons absorbed by the $\cdot\text{OH}$ precursor represents initially 94.2% of the total photon absorption in multi-component mode. However, as the organics are degraded, the fraction of photon absorbed by H_2O_2 constantly increases and H_2O_2 can also be assumed to be the only absorbing species in the $\text{UV/H}_2\text{O}_2$ system in the model.

In homogeneous systems, the LVRPA is a function of position (r , z) and time (t):

$$\text{LVRPA} = \text{LVRPA}(r, z, t) \quad (4)$$

where r and z are the radial and axial coordinates respectively.

As the concentration of H_2O_2 is two orders of magnitude higher than the organics, the concentration of H_2O_2 was assumed to remain constant over the time of irradiation, and therefore the LVRPA becomes independent of time:

$$\text{LVRPA} = \text{LVRPA}(r, z) \quad (5)$$

Based on the equations described by Zalazar et al. [6] and the assumption made in this work, the LVRPA spatial distribution can be described using the one-dimensional model as follows:

$$LVRPA(r, z) = \kappa_H X I(\eta r, z) X \exp(-\kappa'_H X \delta^*) \quad (6)$$

where κ_H and κ'_H are the decadic and naperian absorption coefficients of H_2O_2 respectively (in m^{-1}) which are the product of the decadic/naperian molar absorption coefficient ζ and the concentration of H_2O_2 , $I(\eta r, z)$ is the incident photon flux entering the inner wall of the reactor (in $W m^{-2}$) and δ^* is the dimensionless reaction space radial coordinate (Fig. 1).

In heterogeneous systems the transport of photons is governed by absorption, scattering and emission [15]. The Six-Flux Absorption-Scattering Model (SFM) developed by Brucato et al. [17] has been successfully applied to annular photoreactors [15] and was used in this study. The main assumptions made in this model are: the TiO_2 particles are uniformly distributed in solution, the optical characteristics are constant independently of space and time, the absorption of energy by the fluid and reactor wall are neglected, the photons with energy greater than TiO_2 band-gap are either absorbed or scattered and scattering follows one of the six directions of the Cartesian coordinates [15]. The LVRPA at a point (r, z) in the reactor space for an infinitely long annular photocatalytic reactor is:

$$\begin{aligned} LVRPA = & \frac{\tau_{app} \times I_{(\eta R), z^*}}{\omega_{corr}(1 - \gamma)(1 - \eta)\bar{R}} \times \frac{\eta}{[\eta + (1 - \eta)\delta^*]} \\ & \times [(\omega_{corr} - 1 + \sqrt{1 - \omega_{corr}^2}) \exp^{-\tau_{app}\delta^*} \\ & + \gamma(\omega_{corr} - 1 - \sqrt{1 - \omega_{corr}^2}) \exp^{\tau_{app}\delta^*}] \end{aligned} \quad (8)$$

A detailed description of the model can be found in Li Puma et al. [5] or in supplementary data.

2.6. Electrical energy per order

The electrical energy consumption currently represents the main part of the overall operating cost of AOPs and its evaluation is essential in order to evaluate the economic viability of a process. A figure of merit named electrical energy per order (EEo) has been introduced by Bolton et al. [18] which is defined as the electrical energy (in kWh) required to degrade a given volume of a pollutant, typically $1 m^3$, by one order of magnitude, and is expressed in $kWh m^{-3}$. The EEo is optimally used for low concentration of pollutant when the overall reaction follows first-order and is calculated from the following equation:

$$EEo = \frac{P \times t}{V_T \times \log(C_i/C_f)} \quad (9)$$

where P is the input power of the lamp (in kW), t is the time of irradiation (in h), V_T is the volume of solution treated (in m^3), C_i and C_f are the initial and final concentrations respectively.

The equation can also be expressed in term of rate constant as described by Bolton and Stefan [19]:

$$EEo = \frac{38.38 \times P}{V_T \times k'} \quad (10)$$

where k' is the pseudo-first order rate constant (in min^{-1}).

In addition, the volumetric reaction rate is:

$$r(V) = k' \times C_0 \times V_T \quad (11)$$

where $r(V)$ is the volumetric reaction rate (in $M s^{-1} m^3$).

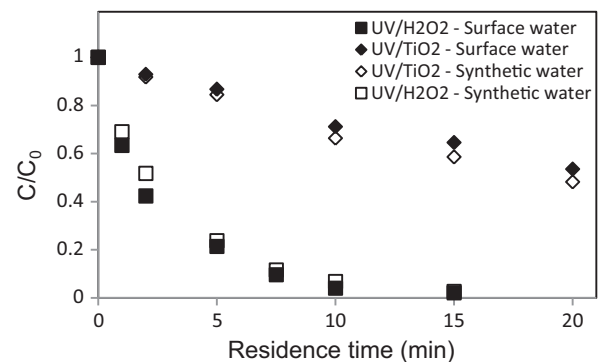


Fig. 2. Degradation of metaldehyde in surface water (black) and synthetic water (white) by UV/ H_2O_2 (square) and UV/ TiO_2 (diamond). $[DOC]=3.5 \text{ mg L}^{-1}$, alkalinity = 120 mg L^{-1} as $CaCO_3$, $[H_2O_2]=8 \text{ mM}$, $[TiO_2]=100 \text{ mg L}^{-1}$, $[metaldehyde]=5.68 \times 10^{-8} \text{ M}=10 \mu\text{g L}^{-1}$.

The rearrangement of Eqs. (10) and (11) enables to express the EEo in function of the reaction rate, such as:

$$EEo = \frac{0.64 \cdot 10^{-3} \times C_0 \times P}{(V_T/V_R) \times r(V)} \quad (12)$$

where EEo is in $kWh m^{-3}$, P in kW , C_0 in M and r in $M s^{-1} m^3$.

3. Results and discussion

Control experiments were carried out to ensure that no direct photolysis or dark adsorption occurred in the systems. The degradation of metaldehyde and the three NOM surrogates in multicomponent mixture achieved no more than 4% removal at a 10 min residence time when neither TiO_2 nor H_2O_2 was added to the system (Supplementary Fig. S1). Dark adsorption of the mixture on TiO_2 over a period of two hours indicates that none of the compounds readily adsorb onto TiO_2 surface (Supplementary Fig. S2). Therefore, as direct photolysis and adsorption do not occur in any of the systems, $^{*}OH$ attack is the only route of degradation.

3.1. Comparison of metaldehyde degradation by UV/ H_2O_2 and UV/ TiO_2 in natural and synthetic waters

More than 90% metaldehyde removal was achieved at a 7.5 min residence time in the UV/ H_2O_2 system for both natural and synthetic waters in the presence of background organic matter and alkalinity (Fig. 2). In contrast, less than 50% removal was achieved at a 20 min residence time in the UV/ TiO_2 system. These low removals by UV photocatalysis are in accordance with a previous study which showed the inhibitor effect of alkalinity on metaldehyde degradation due to the formation of large TiO_2 aggregates increasing the size from $3.5 \mu\text{m}$ without alkalinity to $400 \mu\text{m}$ when carbonate ions were added reducing the surface area of TiO_2 by a factor 150 [9]. The profiles in natural and synthetic waters with similar characteristics showed no major differences in metaldehyde degradation (Fig. 2). Such results suggest that the use of synthetic water accurately represents the reactions occurring in natural water and offers the possibility to follow the degradation of all the species in solution which can give important information on the competition between the micropollutant and other water constituents. As alkalinity had a significant impact on metaldehyde removal by UV/ TiO_2 , simulation are carried out both in the presence and absence of alkalinity to evaluate the extent of this impact and to estimate what could be achieved if a pre-treatment able to break the aggregates was used.

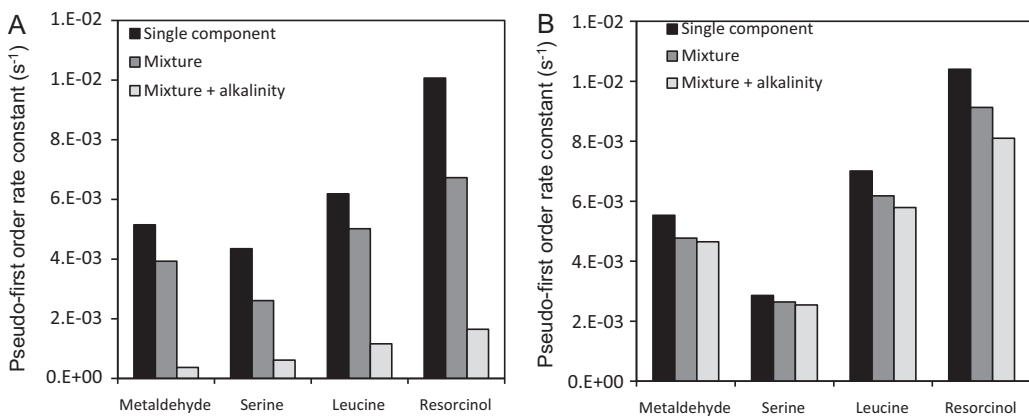


Fig. 3. Degradation of metaldehyde, serine, leucine and resorcinol in single component and in multicomponent mixture in the absence and presence of carbonate ions by (A) UV/TiO₂ and (B) UV/H₂O₂. Alkalinity = 120 mg L⁻¹ as CaCO₃. [TiO₂] = 100 mg L⁻¹, [H₂O₂] = 8 mM UV-C radiation, initial concentrations (μM): [metaldehyde] = 0.0568; [leucine] = [serine] = [resorcinol] = 18.94.

3.2. Degradation kinetics of metaldehyde in single and multi-component mode

Metaldehyde was well degraded by both processes when no competing species were present in solution (Fig. 3A and B). At a 10 min residence time, 95% and 96% of metaldehyde removal were achieved by UV/TiO₂ and UV/H₂O₂ respectively which resulted in first order rate constants of 5.17×10^{-3} and $5.48 \times 10^{-3} s^{-1}$ in accordance with bench scale tests where the first order rate constants were 4.29×10^{-3} and $4.78 \times 10^{-3} s^{-1}$ indicating that rate data can be effectively transferred from bench to pilot plant operation. The presence of competitive species reduced the degradation of metaldehyde by both processes (Fig. 3A and B). The irradiation of TiO₂ led to the partial degradation of the four compounds with associated pseudo-first order rate kinetics in the order resorcinol > leucine > metaldehyde > serine. For instance, the rate of degradation of resorcinol was $k' = 6.73 \times 10^{-3} s^{-1}$ whilst for serine, the least degraded of the four compounds $k' = 2.61 \times 10^{-3} s^{-1}$. Despite being at much lower concentration than the three NOM surrogates, metaldehyde was still removed by the UV/TiO₂ process at a degradation rate of $k' = 3.93 \times 10^{-3} s^{-1}$, compared to $k' = 5.17 \times 10^{-3} s^{-1}$ in single component. The degradation of the multicomponent mixture by UV/H₂O₂ led to faster degradation than by UV/TiO₂ such that the degradation rate for resorcinol was $k' = 9.13 \times 10^{-3} s^{-1}$ and for metaldehyde $k' = 4.77 \times 10^{-3} s^{-1}$ (Fig. 3B). The same sequence of rate constants resorcinol > leucine > metaldehyde > serine was observed. The inhibition of the rate constants in multi-component mode were expected due to the scavenging effect of competing species [20], however the order of degradation does not follow the scavenging

rate of each compound ($k'_{\bullet OH,i} \times [i]$) but the reactivity $k'_{\bullet OH,i}$ as metaldehyde which had a scavenging rate two orders of magnitude lower than serine but a reactivity one order of magnitude higher get removed preferentially in comparison to serine.

Whilst alkalinity had no major effect on the UV/H₂O₂ process (Fig. 3B), the degradation of metaldehyde and the three NOM surrogates was highly affected in the UV/TiO₂ system (Fig. 3A). The presence of alkalinity reduced metaldehyde degradation rate from $k' = 3.93 \times 10^{-3} s^{-1}$ in multi-component mode without alkalinity to $k' = 3.68 \times 10^{-4} s^{-1}$ in multi-component mode with addition of carbonate ions, 93% slower than in the presence of metaldehyde only.

3.2.1. LVRPA radial profiles and VRPA

The LVRPA were different for TiO₂ and H₂O₂ as illustrated by the normalized radial profiles in the middle of the reactor (Fig. 4A). The LVRPA at the reactor wall ($\delta^* = 0$) was significantly higher for UV/TiO₂ in the absence of alkalinity – well dispersed slurry of TiO₂ – than for UV/H₂O₂ at 15285 and 1085 W m⁻³ respectively reflecting the difference in absorption coefficients (Table 2). In the UV/TiO₂ system, more than 80% of the photons emitted by the lamp are absorbed within the first 1/3 of reaction space whilst in the UV/H₂O₂ system only 42% of the emitted photons are absorbed within the entire reaction space. It has been previously demonstrated that more than 80% of the photons reaching the reactor wall were absorbed by the stainless steel material [21,22], which means that a small part of the photons reaching the reactor wall are reflected into the reaction space. Here, the reflected photons have been discarded due to their poor reflection and the lack of reported

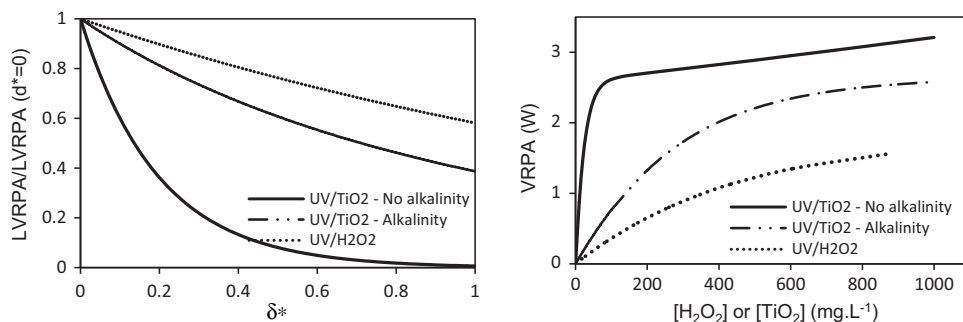


Fig. 4. (A) Normalized radial profiles of the LVRPA in the middle of the reactor ($z^* = 0.5$), as predicted by the radiation models for the conditions in Table 1. LVRPA ($\delta^* = 0$) is 15285, 1239 and 1085 W m⁻³ for UV/TiO₂ without alkalinity, UV/TiO₂ with alkalinity and UV/H₂O₂ systems respectively. (B) Volumetric rate of photon absorption as a function of TiO₂ and H₂O₂ concentrations.

Table 3

Volumetric rate of photon absorption, specific quantum yields and overall quantum yield, electrical energy per order and reaction rate constant independent of photon absorption in the different configurations tested.

	UV/TiO ₂ No alkalinity	UV/TiO ₂ With alkalinity	UV/H ₂ O ₂ No alkalinity	UV/H ₂ O ₂ With alkalinity
VRPA (W)	2.615	0.765	0.828	0.828
VRPA (e s ⁻¹)	5.54 × 10 ⁻⁶	1.62 × 10 ⁻⁶	1.75 × 10 ⁻⁶	1.75 × 10 ⁻⁶
Φ _{metaldehyde/single component} (mole e ⁻¹)	5.99 × 10 ⁻⁵	n.a.	2.03 × 10 ⁻⁴	n.a.
Φ _{metaldehyde/multi-component} (mole e ⁻¹)	3.41 × 10 ⁻⁵	2.43 × 10 ⁻⁵	1.75 × 10 ⁻⁴	1.70 × 10 ⁻⁴
Φ _{serine/multi-component} (mole e ⁻¹)	5.62 × 10 ⁻³	4.80 × 10 ⁻³	3.23 × 10 ⁻²	3.11 × 10 ⁻²
Φ _{leucine/multi-component} (mole e ⁻¹)	1.27 × 10 ⁻²	1.54 × 10 ⁻²	7.55 × 10 ⁻²	7.08 × 10 ⁻²
Φ _{resorcinol/multi-component} (mole e ⁻¹)	1.59 × 10 ⁻²	2.18 × 10 ⁻²	0.112	0.100
Φ _{overall/multi-component} (mole e ⁻¹)	0.0342	0.0420	0.220	0.202
EE _o _{single component} (kWh.m ⁻³)	4.9		4.6	
EE _o _{multi component} (kWh m ⁻³)	6.4	41.1	5.3	5.4
k _{T,M} (m ³ e ⁻¹)	0.810	0.432	3.113	3.034

values in the literature, which leads to a slight underestimation of the true VRPA in the UV/H₂O₂ system.

The presence of alkalinity greatly reduced the rate of photon absorption in the UV/TiO₂ system with LVRPA = 1239 W m⁻³ at z = 0.5 and δ* = 0. As larger aggregates are in solution, the slurry is not as well dispersed and a much larger part of the photons is not absorbed by TiO₂ agglomerates such that only 61% of the photons emitted are absorbed throughout the entire reactor volume (Fig. 4A).

The VRPA of the UV/TiO₂ system was 2.5 times larger than in the UV/H₂O₂ system at 2.61 W (Table 3). Aggregation of the catalyst particles reduced the VRPA of UV/TiO₂ to 0.77 W such that it became slightly lower than the 0.83 W for the UV/H₂O₂ system. Increasing the catalyst dose enhanced the VRPA in both the presence and absence of alkalinity. In the absence of alkalinity catalyst doses up to 100 mg L⁻¹ significantly increased the VRPA beyond which only minor enhancements were observed. In contrast, aggregation of the catalyst in the presence of alkalinity meant that the VRPA was enhanced up to dose of 600 mg L⁻¹ beyond which the VRPA did not increase (Fig. 4B). As alkalinity has no influence on H₂O₂ molecules properties or on the transmissivity of the water, the presence of alkalinity had no impact on the VRPA for the UV/H₂O₂ process which constantly increases with the increase of [H₂O₂] as more photons are absorbed by the solution. At the optimum dose of H₂O₂ (8 mM) the VRPA was 0.83 W which represents a 64% reduction compared to the UV/TiO₂ system even when alkalinity is present. The cost of H₂O₂ plus its own •OH scavenging properties mean that practical economic limits around 27 mg L⁻¹ (0.8 mM) have been suggested [23] and at these levels the VRPA is 0.11 W, 24 times smaller than for UV/TiO₂ demonstrating that the latter is a more effective process at absorbing photons.

3.2.2. Quantum yields

The impact of differences in VRPA on the efficiency of the process, as defined by the quantum yield, was determined by Eq (2) and the initial rates of degradation observe in the pilot trials. In single component mode, the quantum yield for metaldehyde was 5.99 × 10⁻⁵ and 2.03 × 10⁻⁴ mole e⁻¹ for the UV/TiO₂ and UV/H₂O₂ systems respectively. The efficiency of 0.020% for the UV/H₂O₂ was higher than the 0.006% observed for the UV/TiO₂ system indicating the former was more efficient at using the absorbed photons as the rates of degradation were similar but the VRPA was lower. The presence of NOM reduced the quantum yield of metaldehyde by 43% for UV/TiO₂ and 14% for UV/H₂O₂ but increased overall quantum yield to 3.42% and 22.0% respectively indicating better utilization of the available photons when more material is available for reaction.

Both the rates of degradation of metaldehyde and NOM surrogates and the VRPA were severely affected by the presence of alkalinity in the UV/TiO₂ process. Interestingly, as the VRPA was more affected than the rates of degradation, the overall quantum yield was slightly greater in the presence of alkalinity. On the other

hand, it had no major impact on the quantum efficiency of the UV/H₂O₂ system – 22.0 and 20.2% in the absence and presence of alkalinity respectively.

The quantum yield is proportional to the initial rate of degradation and as metaldehyde is present at concentrations 3 orders of magnitude lower than the background organic matter, the individual quantum yields of metaldehyde are very low for both processes and represent only 0.058% and 0.084% of the overall quantum yields for UV/TiO₂ ad UV/H₂O₂ respectively in the presence of both NOM surrogates and carbonate ions (Table 3). The overall quantum yields observed here are in the order of efficiencies previously reported [6,15] and the efficiency is 5 times higher for UV/H₂O₂ than for UV/TiO₂.

3.2.3. Electrical energy consumption

In single component mode, both processes exhibit similar EE_o of 4.9 and 4.7 kWh m⁻³ for UV/TiO₂ and UV/H₂O₂ respectively (Table 3). The presence of background organic matter increased the EE_o by 16% for UV/H₂O₂ whilst that of UV/TiO₂ increased more significantly by 31%. More importantly, no difference was observed for UV/H₂O₂ when carbonate ions were added, the same action increased the EE_o of the UV/TiO₂ system by 540% with values becoming more than 7.5 times greater for UV/TiO₂ than for UV/H₂O₂. Crittenden et al. [24] reported that EE_o values of 2.65 kWh m⁻³ or less were considered favourable. Here, the values reported are slightly higher, however the scale-up from bench scale to full scale is known to decrease the EE_o by at least one order of magnitude [25] and hence, the degradation of metaldehyde by both processes would require less than 1 kWh m⁻³ and demonstrates the potential to be economically viable.

However, these values have to be balanced as although the electrical energy consumption represents the main cost of AOPs, other parameters also need to be considered especially the cost of chemicals. In this study, optimum concentrations of •OH precursors have been used, e.g. 100 mg L⁻¹ and 8 mM for TiO₂ and H₂O₂ respectively. Such concentration of H₂O₂ appears economically unrealistic for full scale plants, and a reduction of this concentration to 0.8 mM would result in an EE_o = 139.1 kWh m⁻³. Moreover, the high EE_o values found for the UV/TiO₂ system are essentially due to the presence of alkalinity which leads to the formation of large TiO₂ aggregates. Breaking these aggregates would lead to greater surface area available and potentially to better rates of degradation, reducing the EE_o (theoretically down to values obtained in the presence of NOM surrogates only). However, energy would be required to break the aggregates which adds up to the need of a post-photocatalysis filtration system to separate the treated water from the catalyst which is recirculated in the system.

3.2.4. Rate constant independent of photon absorption

The rate constants determined in research studies are often specific to the reactor set-up and geometry as they are not decoupled

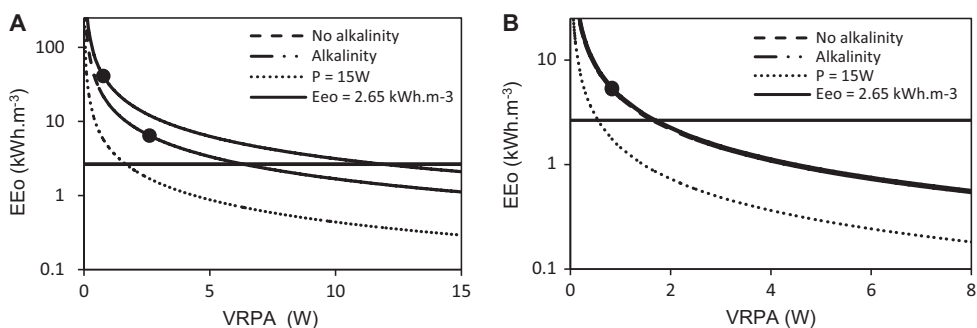


Fig. 5. Influence of VRPA, alkalinity and lamp power on the electrical energy requirement for the degradation of metaldehyde by (A) UV/TiO₂ and (B) UV/H₂O₂. * represent the values obtained in this study. The dash line represents a scenario where a similar VRPA is reached with a 15 W lamp instead of the 45 W lamp used in the study.

from the amount of radiation absorbed by the system [15]. As the degradation kinetics of metaldehyde follows pseudo-first order, the reaction rate can be modelled by:

$$-r_M = k_{T,M}(LVRPA)^m C_M \quad (13)$$

where $k_{T,M}$ is the apparent reaction rate constant of metaldehyde degradation independent of photon absorption. In UV/TiO₂ photocatalysis, the rate of reaction is proportional to the radiant flux Φ up to 25 mW cm⁻² after which it becomes proportional to $\Phi^{1/2}$ due to the predominance of e⁻–h⁺ recombination over photoreaction [26]. Here, the light intensity emitted by the lamp is 14.1 mW cm⁻² and therefore linear relationship exists between r and LVRPA, resulting in $m=1$ (always 1 in the case of UV/H₂O₂).

In order to enable the model to be used for continuous and recirculation systems, the rate equations and the material balance were combined and yielded:

$$V_T \frac{dC_M}{dt} = k_{T,M} \times C_M \times \int_{V_R} (LVRPA)^m dV_R \quad (14)$$

which after integration becomes:

$$\ln \frac{C_M}{C_{0,M}} = -\frac{k_{T,M} \times \int_{V_R} (LVRPA)^m dV_R}{V_T} \times t = k'_M \times t \quad (15)$$

As $m=1$ in the study:

$$\int_{V_R} (LVRPA)^m dV_R = VRPA \quad (16)$$

and finally:

$$k_{T,M} = \frac{k'_M \times V_T}{VRPA} \quad (17)$$

The rate constants $k_{T,M}$ found here (Table 3) can therefore be applied to any reactor configuration with the condition that the radiant flux of the system is <25 mW cm⁻² for UV/TiO₂. The values obtained in the presence of both background organic matter and alkalinity should represent the degradation of metaldehyde in surface water containing 3.5 mg L⁻¹ DOC and an alkalinity of 120 mg L⁻¹ as CaCO₃.

By combining Eqs. (11), (12) and (17), a relationship between EEo, P, k_T and VRPA is obtained, such that:

$$EEo = \frac{0.64 \cdot 10^{-3} \times P}{k_T \times VRPA} \quad (18)$$

As already observed above, the alkalinity substantially increases the energy requirement of UV/TiO₂ whilst it does not impact UV/H₂O₂ (Fig. 5). In fact, the presence of alkalinity reduces the rate of photon absorbed in the system (VRPA) and ultimately results in higher EEo. Consideration of equation (18) suggests that the

required VRPA to achieve the target EEo of 2.65 kWh m⁻³ is 1.69 W and 6.33 W for UV/H₂O₂ and UV/TiO₂ systems based on the 45 W lamp used in the current study. Reduction of the lamp power to 15 W reduces the required VRPA to 0.55 and 2.15 respectively. In the set up used in the current work the required EEo was obtained when an optimum concentration was used (0.8 mM) but is considerably greater than the 0.106 W obtained at more practical concentrations. Consequently improvements in reactor design that ensure greater utilization of the transmitted photons are required to ensure economic viability. Such improvement can be achieved by either increasing the reactor channel width to 11.7 cm and/or incorporating new reflecting materials for the inner wall of the reactor such as aluminium which is known to reflect UV light [27]. In contrast, improvements in the TiO₂ system require that the audit of catalyst is held within the reactive volume and so preferences narrower channel widths of 9 mm associated with longer reactors (in this case 90 cm for a similar reactor volume). Finally, a new source of UV light, UV light emitting diodes (UV-LEDs) have shown great potential in replacing traditional Hg lamps [28] and although at this stage of development they exhibit low output power and low wall plug efficiency, they are predicted to become soon competitive with Hg lamps and should outperform them within 6–8 years [29] and hence could result in significant savings in electrical energy consumption.

4. Conclusion

Both background DOC and alkalinity have an inhibitory effect on the reaction rate of metaldehyde and therefore on EEos, especially for UV/TiO₂ where the alkalinity is a major issue and a chemical or physical process needs to be used to break the TiO₂ aggregates. Moreover, although more photons are absorbed by TiO₂ than H₂O₂, the UV/H₂O₂ process remains more effective in term of quantum yield and energy consumption. The optimization of reactor design, TiO₂ particles properties, and efficiency of light sources will ultimately reduce the energy consumption and bring AOPs as contenders for new drinking water treatment processes.

Acknowledgement

The authors would like to express their gratitude for the financial support for this project by Severn Trent Water Ltd.

Appendix A. Supplementary data

Supplementary data associated with this article can be found, in the online version, at <http://dx.doi.org/10.1016/j.apcatb.2013.02.045>.

References

- [1] V.J. Pereira, H.S. Weinberg, K.G. Linden, P.C. Singer, Environmental Science and Technology 41 (2007) 1682–1688.
- [2] I.A. Katsoyiannis, S. Canonica, U. von Gunten, Water Research 45 (2011) 3811–3822.
- [3] M.L. Satuf, J. Brandi, A.E. Cassano, O.M. Alfano, Catalysis Today 129 (2007) 110–117.
- [4] G. Li Puma, P.L. Yue, Industrial and Engineering Chemistry Research 38 (1999) 3238–3245.
- [5] G. Li Puma, B. Toepfer, A. Gora, Catalysis Today 124 (2007) 124–132.
- [6] C.S. Zalazar, M.L. Satuf, O.M. Alfano, A.E. Cassano, Environmental Science and Technology 42 (2008) 6198–6204.
- [7] E.J. Rosenfeldt, K.G. Linden, Environmental Science and Technology 41 (2007) 2548–2553.
- [8] W. Song, V. Ravindran, M. Pirbarazi, Chemical Engineering Science 63 (2008) 3249–3270.
- [9] O. Autin, J. Hart, P. Jarvis, J. MacAdam, S.A. Parsons, B. Jefferson, Water Research 47 (2013) 2041–2049.
- [10] G. Xu, M.R. Chance, Analytical Chemistry 77 (2005) 4549–4555.
- [11] D. Minakata, K. Li, P. Westerhoff, J. Crittenden, Environmental Science and Technology 43 (2009) 6220–6227.
- [12] Chemspider, 2012. Chemical data base search, Available at <http://www.chemspider.com> (accessed February 2012).
- [13] M.I. Cabrera, O.M. Alfano, A.E. Cassano, Journal of Physical Chemistry 100 (1996) 20043–20050.
- [14] M. Salaises, B. Serrano, H.I. de Lasa, Chemical Engineering Journal 90 (2002) 219–229.
- [15] G. Li Puma, V. Puddu, H.K. Tsang, A. Gora, B. Toepfer, Applied Catalysis B: Environmental 99 (2010) 388–397.
- [16] O. Autin, J. Hart, P. Jarvis, J. MacAdam, S.A. Parsons, B. Jefferson, Water Research 46 (2012) 5655–5662.
- [17] A. Brucato, A.E. Cassano, F. Grisafi, G. Montante, L. Rizzuti, G. Vella, AIChE Journal 52 (2006) 3882–3890.
- [18] J.R. Bolton, K.G. Bircher, W. Tumas, C.A. Tolman, Pure and Applied Chemistry 73 (2001) 627–637.
- [19] J.R. Bolton, M.I. Stefan, Research on Chemical Intermediates 28 (2002) 857–870.
- [20] W.R. Haag, J. Hoigné, Chemosphere 14 (1985) 1659–1671.
- [21] I. Nicole, J. De Laat, M. Dore, J.P. Duguet, C. Bonnel, Water Research 24 (1990) 157–168.
- [22] J.R. Bolton, Water Research 34 (2000) 3315–3324.
- [23] A. Hirvonen, T. Tuukkanen, M. Ettala, S. Korhonen, P. Kalliokoski, Environmental Technology 19 (1998) 821–828.
- [24] J.C. Crittenden, S. Hu, D.W. Hand, S.A. Green, Water Research 33 (1999) 2315–2328.
- [25] S.A. Parsons, Advanced Oxidation Processes for Water and Wastewater Treatment, IWA, UK, 2004.
- [26] J.-M. Herrmann, Topics in Catalysis 34 (2005) 49–65.
- [27] J. Fu, M. Ji, Z. Wang, L. Jin, D. An, Journal of Hazardous Materials 131 (2006) 238–242.
- [28] S. Vilhunen, J. Puton, J. Virkutyte, M. Sillanpää, Environmental Technology 32 (2011) 865–872.
- [29] M.A.S. Ibrahim, B. Jefferson, J. MacAdam, Commercial evaluation of UV-LED in water treatment applications, MSc thesis, Cranfield University, UK, 2012.